

1 Mapping key soil micronutrients across the Tibetan Plateau

2 Huangyu Huo^{1,2}, Xiling Gu^{1,2}, Jiayi Li^{1,2}, Shanshan Yang¹, Yafeng Wang^{1*}, Jinzhi Ding^{1*}

3 ¹State Key Laboratory of Tibetan Plateau Earth System, Environment and Resources (TPESER), Institute of Tibetan Plateau
4 Research, Chinese Academy of Sciences, Beijing 100101, China.

5 ²University of Chinese Academy of Sciences, College of Resources and Environment, Beijing 100049, China.

6 *Corresponding to: Jinzhi Ding (jzding@itpcas.ac.cn), Yafeng Wang (yfwang@itpcas.ac.cn)

7 **Abstract.** Soil micronutrient supply sustains critical ecological functions but exhibit poorly quantified distribution patterns in
8 high-altitude ecosystems. This study bridges this knowledge gap through a large-scale investigation across the Tibetan Plateau,
9 a cold-arid region where cryogenic weathering, aridity, and suppressed pedogenesis interact to govern micronutrient cycling.
10 We assembled a plateau-wide dataset from 526 sites with triplicate surface soils (0-10 cm) per site (n = 1,660). Four
11 micronutrients (Fe, Mn, Zn, and V) were measured and paired with multi-source predictors (climate, vegetation, soil covariates,
12 topography, grazing disturbance, and weathering proxy). Elemental contents span broad ranges, with site-level summaries
13 (mean \pm SD, mg·kg⁻¹) of Fe 22,864.30 \pm 7,589.01, Mn 576.74 \pm 206.44, Zn 27.24 \pm 8.55, and V 56.99 \pm 19.33. Random Forest
14 model was employed to quantify controls and generate high-resolution spatial maps. Key results reveal that pronounced
15 regional heterogeneity is driven primarily by weathering intensity with secondary modulation from climate and topography
16 covariates. Element-specific spatial patterns were observed, with Fe enrichment in southeastern/southern plateau, Mn
17 gradients increasing southeastward. Zn hotspots in central-eastern and western marginal zones, and V exhibits a moderate
18 spatial gradient, with higher contents in the southeastern Tibetan Plateau and relatively lower values in the northwest. We
19 provide 1-km maps of all four micronutrients together with pixel-wise uncertainty layers to support benchmarking of
20 process-based micronutrient cycling models and to inform sustainable ecosystem management under climate change. The
21 dataset is openly available at TPDC (<https://doi.org/10.11888/Terre.tpdc.303242>; Huo et al., 2025).

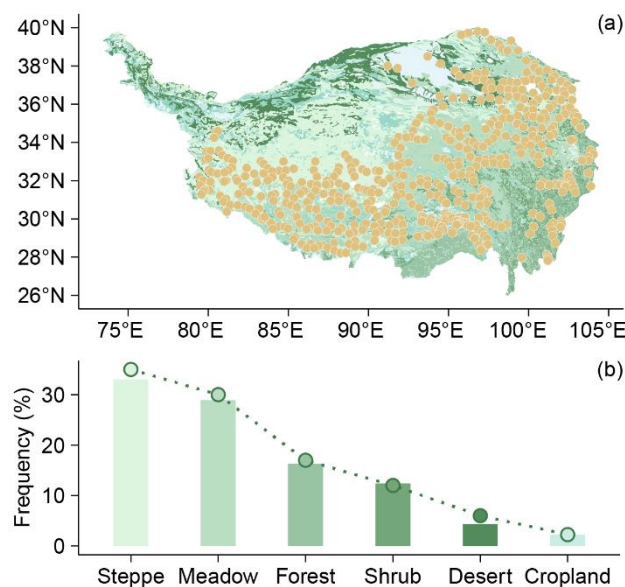
23 **1 Introduction**

24 As essential yet trace-level components of living systems, micronutrients (e.g., Fe, Mn, Zn, and V) sustain fundamental
25 ecological processes, including photosynthesis (Fe, Mn; Fischer et al., 2015; Schmidt et al., 2020), respiration (Fe; Dallman,
26 1986), enzymatic/redox functions (Zn, V; Hänsch et al., 2009), and biological nitrogen fixation (V; O'Hara, 2001). Crucially,
27 micronutrient gradients in soils propagate through trophic chains, directly influencing human nutrition and health;
28 deficiencies exacerbate global malnutrition burdens (Fageria et al., 2002; White et al., 2005). Despite their pivotal role in
29 ecosystem stability and food security (Presteele et al., 2016; Stehfest et al., 2019), critical knowledge gaps persist regarding
30 the distribution patterns and drivers of soil micronutrients from regional to global scales.

31 The Tibetan Plateau represents a uniquely important yet underrepresented region for addressing these knowledge gaps. As
32 the high-altitude landmass and the most extensive alpine permafrost region at low to mid-latitude (Yao et al., 2012), the
33 Tibetan Plateau supports vast areas of cold- and nutrient-limited ecosystems, where plant productivity, microbial activity, and
34 biogeochemical cycling are particularly sensitive to micronutrient availability (Han et al., 2022; Tian et al., 2019). In such
35 environments, micronutrients may act as co-limiting or even primary limiting factors alongside nitrogen and phosphorus, yet
36 their spatial distributions and environmental controls remain poorly quantified (Dong et al., 2023; Pan et al., 2024).
37 Moreover, the Tibetan Plateau is experiencing rapid climate change characterized by accelerated warming and increasing
38 moisture availability, which is expected to fundamentally alter soil weathering regimes, redox conditions, and
39 mineral-organic interactions (Yu et al., 2024; Cheng et al., 2024). Without robust baseline assessments of soil micronutrients,
40 it remains difficult to evaluate how ongoing climate change may reshape nutrient limitation patterns and ecosystem
41 functioning across high-altitude regions.

42 Soil micronutrient supply originates from coupled physicochemical weathering and biological mediation, critically regulated
43 by local climate and topography (Ochoa-Hueso et al., 2020; Hartmann et al., 2023). In cold-arid high-altitude regions,
44 particularly the Tibetan Plateau, extreme environmental interactions uniquely govern micronutrient cycling. Cryogenic
45 processes such as glacial erosion and freeze-thaw cycles, accelerate physical bedrock weathering to mobilize lithogenic
46 micronutrient reservoirs, while aridity concurrently constrains chemical weathering and elemental release (Mu et al., 2020;
47 Mu et al., 2016). Low temperatures suppress biological turnover and synergize with aridity to compromise pedogenesis
48 through clay deficits and diminished mineral reactive sites, thereby reducing elemental retention capacity (Dijkstra et al.,
49 2004). The combined effects of these opposing processes jointly determine the overall abundance and spatial heterogeneity
50 of soil micronutrients across alpine soils, likely differing from the patterns of soil micronutrients observed in temperate and
51 tropical regions.

52 Despite the ecological significance of soil micronutrient, our understanding of their spatial distribution and controlling
53 factors across the Tibetan Plateau remains limited. Previous studies have been largely confined to localized transects or
54 site-specific investigations (e.g., the Heihe River Basin and the Tibetan Plateau Highway), offering limited spatial coverage
55 and representativeness, and providing insufficient insight into how climate, vegetation, topography and lithology jointly
56 regulate micronutrient patterns at the regional scale (Zhang et al., 2012; Guan et al., 2017; Bu et al., 2016). To address these
57 knowledge gaps, we conducted a large-scale field investigation across the Tibetan Plateau, establishing 526 sampling sites
58 distributed across representative temperature and moisture gradients (**Fig. 1**). The sampling design encompassed the plateau's
59 dominant vegetation types and lithological classes. Using this dataset, we analyzed distribution patterns and key controlling
60 factors for four essential micronutrients (Fe, Mn, Zn, V). We then applied a Random Forest algorithm to generate
61 high-resolution spatial distribution maps of these micronutrients, representing the first comprehensive quantification at this
62 scale and resolution.



63
64 **Figure 1.** Sampling strategy and ecosystem representativeness. (a) Spatial distribution of sampling sites superimposed on China's
65 1:1,000,000 vegetation map. (b) Areal proportions of ecosystem types (bars) versus sampling point frequency distribution (dots) across
66 corresponding ecosystems. Similar bar and dot heights indicate that the sampling is proportionally representative.

67 2 Methods

68 2.1 Field survey and soil micronutrients analysis

69 We analyzed 1,660 topsoil samples collected from 526 locations during a 2019-2021 growing season (July-August) field
70 survey across the Tibetan Plateau (79-105°E, 27-40°N; **Fig. 1a**). Sampling sites represent major plateau ecosystems: forests,
71 shrubs, steppes, meadows, deserts, and croplands (**Table 1**). Our field sampling followed a proportional, area-weighted

72 design, whereby the number of sampling sites allocated to each ecosystem type was approximately proportional to its areal
73 extent across the Tibetan Plateau. This design aims to provide a plateau-wide, regionally representative characterization of
74 surface-soil micronutrients across dominant ecosystem types. The sites span broad environmental gradients, ranging from
75 759 to 5565 m in elevation, -7.83 to 18.46 °C in mean annual temperature (MAT), and 23 to 898 mm in mean annual
76 precipitation (MAP), effectively capturing the plateau's topographic and climatic variability. Site was selected using
77 standardized criteria: maintaining relative homogeneity in species composition, community structure, and habitat conditions,
78 and avoiding proximity to roads or areas with frequent human activity. At each site, we established a 10×10 m² quadrat and
79 collected triplicate soil samples along the diagonal at three positions (0 m, 7.1 m, and 14.1 m; 0-10cm depth), corresponding
80 to the start, midpoint, and end of the quadrat diagonal. This design allows sampling across the spatial heterogeneity within
81 each plot while maintaining a standardized sampling framework. This depth was chosen because it represents the
82 biologically active surface horizon most relevant to plant uptake and microbially mediated cycling, and is widely used in
83 regional soil inventories for comparability across ecosystems (Du et al., 2017; Cardon et al., 2013). This consistent protocol
84 ensures cross-site comparability while capturing the variability of surface layer that most strongly interacts with vegetation
85 and climate. Geographic coordinates, elevation, community type, and species composition (Cheng et al., 2022) were
86 systematically documented.

87 To ensure the reliability of soil micronutrient measurements, we adopted a two-step analytical strategy. First, all 1,660
88 topsoil samples collected from 526 sampling locations were air-dried, sieved (2 mm), and analyzed in the laboratory using a
89 third-generation X-ray fluorescence spectrometer (XRF). All micronutrient data reported in this study are based on these
90 laboratory XRF measurements. Second, to independently validate the XRF-derived concentrations, a subset of 218 samples
91 was randomly selected and re-analyzed using inductively coupled plasma-mass spectrometry (ICP-MS), a widely accepted
92 reference method for elemental analysis (Simon, 2005). Among the examined elements, Fe ($R^2 = 0.81$), Mn ($R^2 = 0.67$), Zn
93 ($R^2 = 0.49$), and V ($R^2 = 0.77$) exhibit clear and statistically significant linear relationships with ICP measurements,
94 demonstrating moderate to strong correlation (**Fig. S1**). The increased dispersion observed at low contents reflects known
95 limitations of XRF near detection thresholds, rather than method failure. Moreover, our analytical strategy follows
96 established practice in large-scale geochemical mapping, where XRF is commonly used for high-throughput determination
97 of total/major-element composition, while ICP-based methods are commonly employed in parallel for complementary
98 measurements (e.g., extracted fractions, waters, or elements requiring lower detection limits) and, where appropriate, for
99 inter-method comparison and validation. In addition to GEMAS and the NGSAs, similar XRF-based workflows have been
100 implemented in other regional/national baseline programmes (e.g., BGS G-BASE in the UK, the FOREGS Geochemical

101 Atlas of Europe, and the Global Geochemical Baselines framework). These precedents support the robustness and suitability
 102 of using XRF with targeted ICP verification for plateau-scale geochemical datasets (Table S1).

103 **Table 1.** Ecosystem classification and sampling coverage on the Tibetan Plateau.

Biome	Characteristics and dominant plant species	elevation ranges	climate conditions (temperature/precipitation)	No. of samples	No. of locations
Steppe	Alpine steppes, dominated by cold-adapted herbaceous species such as <i>Stipa purpurea</i> , features sparse vegetation adapted to cold-arid conditions.	1961-5151 m	-7.1-8.0 °C; 34.32-785.61 mm	569	180
Meadow	Alpine meadows feature dense, low-stature vegetation sustained by year-round low temperatures, high humidity, and water-retentive soils. These ecosystems thrive on gentle slopes and valley floors at higher elevations, hosting relatively diverse flora with characteristic dominance of sedges including <i>Kobresia pygmaea</i> and <i>K. humilis</i> .	2661-5565 m	-7.8-9.2 °C; 158.42-848.70 mm	499	154
Forest	Forests on the Tibetan Plateau concentrate primarily in the southeastern region, dominated by high-altitude cold-temperate coniferous forests. These humid-adapted ecosystems feature <i>fir (Abies)</i> and <i>spruce (Picea)</i> species as characteristic components.	1453-4237 m	-0.6-16.5 °C; 400.34-898.48 mm	265	87
Shrub	Tibetan shrublands primarily occur in arid and alpine zones, characterized by low-growing, drought-tolerant dwarf shrubs such as <i>Lonicera (honeysuckle)</i> and <i>Rhododendron</i> species adapted to nutrient-poor soils and extreme climatic conditions.	2169-5022 m	-5.2-11.8 °C; 301.40-868.63 mm	190	64
Desert	Alpine deserts occur in extremely arid, cold regions and exhibit extremely sparse vegetation dominated by <i>arid-tolerant dwarf shrubs</i> and <i>herbs</i> .	2108-5158 m	-7.1-5.6 °C; 22.64-443.43 mm	101	29
Cropland	Cropland, concentrated in river valleys and basin floors and is dominated by highland barley (<i>Hordeum vulgare</i> var. <i>nudum</i> , “qingke”), with spring wheat (<i>Triticum aestivum</i>), rapeseed (<i>Brassica napus</i>), and potato (<i>Solanum tuberosum</i>) commonly cultivated; vegetation cover is strongly seasonal and often bare after harvest.	759-4360 m	0.5-18.4 °C; 112.53-783.06 mm	36	12

104 Biomes are grouped by diagnostic characteristics; dominant plant species are italicized. Elevation range gives the minimum-maximum
 105 elevation (m) of sampling sites within each biome. Climate conditions report site-level ranges of mean annual temperature (°C) and mean
 106 annual precipitation (mm). No. of samples is the number of soil samples analyzed (0-10 cm, three replicates per site), and No. of locations
 107 is the number of unique sampling sites.

108 2.2 Soil Properties

109 Soil samples were sifted through 2 mm sieve, discarding visible stones and extracted roots. Soil pH was measured using the
 110 potentiometric method, and soil texture analysis, quantifying clay, silt, and sand content fractions, was determined using a
 111 laser diffraction particle size analyzer (Mastersizer 2000, Malvern, UK). Soil organic carbon (SOC) content was quantified
 112 via the potassium dichromate oxidation method (Walkley-Black) with external heating. The chemical index of alteration

113 (CIA) was calculated using the molar proportions of Al_2O_3 , CaO^* , Na_2O , and K_2O according to the formula: $\text{CIA} = [\text{Al}_2\text{O}_3 /$
114 $(\text{Al}_2\text{O}_3 + \text{CaO}^* + \text{Na}_2\text{O} + \text{K}_2\text{O})] \times 100$ (Fedo et al., 1995). The major-element oxides used to calculate CIA (Al_2O_3 , CaO ,
115 Na_2O and K_2O) were obtained from laboratory XRF measurements, which provide a well-established basis for CIA-based
116 evaluation of relative chemical weathering gradients, and data quality was ensured through standard QA/QC including
117 replicate analyses and certified reference materials. CIA reflects the relative loss of mobile base cations (Ca, Na, K)
118 compared with the enrichment of immobile Al during weathering (McLennan, 1993). Higher CIA values indicate stronger
119 chemical weathering and more advanced soil development, whereas lower values suggest weaker weathering and limited
120 leaching of base cations (Nesbitt et al., 1982).

121 **2.3 Environmental variables**

122 We considered geographic, climatic, biological, and edaphic drivers. Field measurements provided location (longitude,
123 latitude), slope, aspect and vegetation type. For the spatial prediction of micronutrient distributions, however, the gridded
124 predictor variables (e.g., elevation, slope, aspect, vegetation cover) were derived from online datasets in order to upscale
125 site-level observations to the Plateau scale. Slope and aspect data came from the National Tibetan Plateau Data Center
126 (<https://data.tpsc.ac.cn>). The digital elevation model (DEM) data were collected from the Resource and Environment
127 Science and Data Center (<https://www.resdc.cn/>). Climate variables, mean annual temperature (MAT) and mean annual
128 precipitation (MAP) were downloaded from the Climate Data Store (<https://cds.climate.copernicus.eu/#!/home>). The Aridity
129 Index (AI), calculated as mean annual precipitation/mean annual reference evapotranspiration, was obtained from the Global
130 Aridity Index dataset (Trabucco et al., 2018), where higher values indicate greater humidity. Vegetation types (Forest, Shrub,
131 Meadow, Steppe, Desert, Cropland) followed the 1:1,000,000 China Vegetation Map classification (Hou, 2019). The
132 normalized difference vegetation index (NDVI) data were obtained from an Earthdata Search (<https://search.earthdata.nasa.gov/search>). The net primary productivity (NPP) data were obtained from the study by Chen et al. (2023) and
133 were calculated using the CASA model (Potter et al., 1993). The grazing activity data were obtained from statistical
134 yearbooks. Based on the lithological data published by Dijkshoorn et al. in 2018, the rock types on the Tibetan Plateau were
135 classified into acidic igneous rock (IA), acidic metamorphic rock (MA), clastic sedimentary rock (SC), carbonate rock (SO),
136 aeolian facies rock (UE), and fluvial facies rock (UF).

138 **2.4 Relative importance analysis and soil micronutrient mapping**

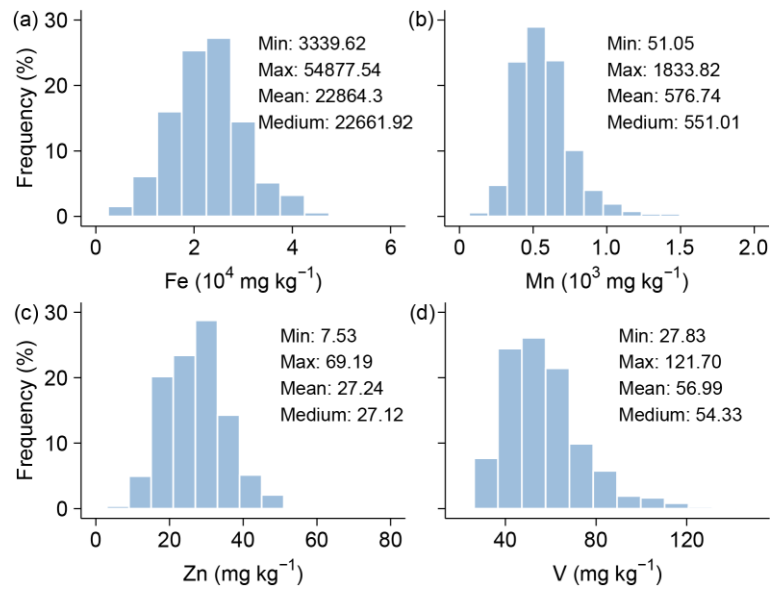
139 Soil micronutrient measurements were preprocessed to detect and remove outliers exceeding the mean ± 3 standard
140 deviations. After data screening, the retained sample sizes are: Fe 1654 (from 1660), Mn 1630 (from 1646), Zn 1655 (from

1661), and V 857 (from 867). To evaluate the relative importance of predictors in explaining soil micronutrient variability across the Tibetan Plateau, we applied the random forest permutation importance (%IncMSE) to independently cross-validate the driver rankings. For spatial prediction, we developed four area-wide random forest models (each comprising 500 trees) targeting Fe, Mn, Zn, and V contents. The models were trained using a suite of environmental predictors, including topographic features (DEM, slope, aspect), climate variables (MAT, MAP, AI), vegetation indices (NDVI, NPP), soil covariates (texture, SOC, pH, CIA), and grazing intensity. Random forest was selected for its ability to model complex, nonlinear relationships and interactions among diverse types of predictors. Model hyperparameters were optimized using grid search combined with tenfold cross-validation. To assess model generalizability, we examined the extent to which the predictor parameter space in the validation set overlapped with that of the original training data. Model performance was evaluated by comparing predicted versus observed values using scatterplots (predicted on the x-axis, observed on the y-axis) following the method of Piñeiro et al. (2008), with models achieving strong predictive performance ($R^2 = 0.6-0.7$). The uncertainty layer is calculated as the inter-pixel variance among tree predictions. All spatial predictions were produced on a uniform 1 km grid (0.01°) across the Tibetan Plateau to maintain consistent spatial support for both predictions and associated uncertainty estimates. All statistical analyses were conducted using R version 3.4.4.

155 **3 Results**

156 **3.1 Soil micronutrients content**

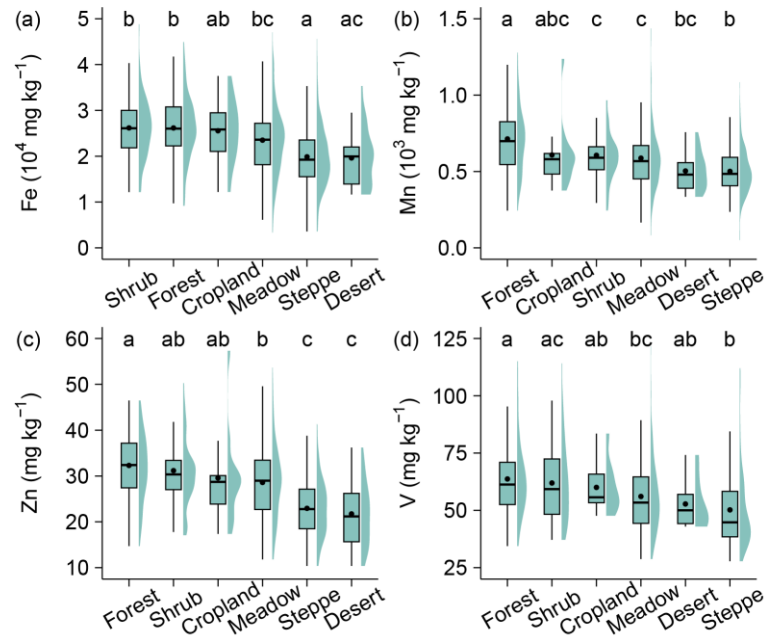
157 Across all sites, soil micronutrient contents varied widely, with mean value of $22,864.30 \pm 7,589.01$ for Fe (mean \pm SD, $\text{mg}\cdot\text{kg}^{-1}$), 576.74 ± 206.44 for Mn, 27.24 ± 8.55 for Zn, and 56.99 ± 19.33 for V. Coefficients of variation ($\text{CV} = \text{SD}/\text{mean}$) were 33% for Fe, 36% for Mn, 31% for Zn, and 34% for V. Collectively, Fe and Mn dominate in absolute abundance, whereas Zn and V occur at tens of $\text{mg}\cdot\text{kg}^{-1}$, indicating heterogeneous but orderly micronutrient levels across the Plateau (**Fig. 2**).



162
163 **Figure 2.** Frequency distributions of soil micronutrients (Fe, Mn, Zn, V) across the Tibetan Plateau.

164 **3.2 Soil micronutrients across vegetation types**

165 Soil micronutrient content (Fe, Mn, Zn, and V) varied significantly among different vegetation types (**Fig. 3**). Fe contents
 166 were highest in shrub and forest ecosystems, with mean values of $26,264.11 \text{ mg}\cdot\text{kg}^{-1}$ and $26,090.66 \text{ mg}\cdot\text{kg}^{-1}$, respectively,
 167 significantly exceeding values observed in desert ($19,762.66 \text{ mg}\cdot\text{kg}^{-1}$) and steppe ecosystems ($19,852.37 \text{ mg}\cdot\text{kg}^{-1}$) by
 168 31-33%. Similarly, Mn contents were significantly higher in forest ($703.22 \text{ mg}\cdot\text{kg}^{-1}$) than in shrub ($606.33 \text{ mg}\cdot\text{kg}^{-1}$),
 169 meadow ($591.59 \text{ mg}\cdot\text{kg}^{-1}$), desert and steppe ecosystems (both below $510 \text{ mg}\cdot\text{kg}^{-1}$). Zn demonstrated a strong
 170 vegetation-dependent variability, with forest ($32.00 \text{ mg}\cdot\text{kg}^{-1}$) exhibiting the highest values and steppe ($22.94 \text{ mg}\cdot\text{kg}^{-1}$) and
 171 desert ($21.95 \text{ mg}\cdot\text{kg}^{-1}$) the lowest, shrub and cropland were intermediate and not significantly different from forest or
 172 meadow. V also varied among vegetation types, with forest being significantly higher than meadow and steppe, and shrub
 173 significantly higher than steppe, whereas cropland and desert displayed intermediate levels.

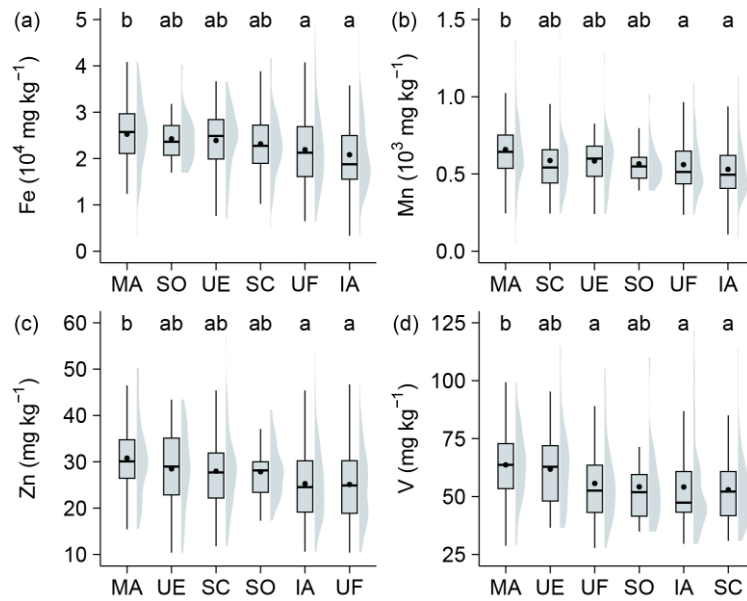


174

175 **Figure 3.** Variability in soil micronutrient contents (Fe, Mn, Zn, V) across Tibetan vegetation types. Boxplots show the data distributions
 176 for each vegetation type. Within each plot, the boxes represent the interquartile range (IQR), the horizontal lines within boxes indicate the
 177 median values, and black dots denote the mean values. The whiskers extend to 1.5 times the IQR. The surrounding shaded violin shapes
 178 indicate the kernel density distribution of the data. Lowercase letters denote significance groups from Tukey's HSD multiple comparisons
 179 ($\alpha = 0.05$): groups sharing at least one letter do not differ significantly, whereas groups with no letters in common differ significantly (e.g.,
 180 "ab" is not different from "a" or "b").

181 **3.3 Soil micronutrients across lithological classes**

182 Lithological class exerted a significant influence on the distribution of several soil micronutrients (**Fig. 4**). Fe contents
 183 differed among lithological classes, with soils derived from acidic metamorphic rocks showing the highest mean value
 184 25,252.72 $\text{mg}\cdot\text{kg}^{-1}$ and being significantly higher than soils developed from acidic igneous rocks (20,830.15 $\text{mg}\cdot\text{kg}^{-1}$) and
 185 fluvial facies rocks (21,910.22 $\text{mg}\cdot\text{kg}^{-1}$), whereas carbonate (24,260.96 $\text{mg}\cdot\text{kg}^{-1}$), eolian facies (23,902.77 $\text{mg}\cdot\text{kg}^{-1}$), and
 186 clastic sedimentary rocks (23,157.66 $\text{mg}\cdot\text{kg}^{-1}$) exhibited intermediate levels and were not significantly different from either
 187 group. A similar pattern was observed for Mn, where acidic-metamorphic-driven soils (658.37 $\text{mg}\cdot\text{kg}^{-1}$) were significantly
 188 higher than acidic-igneous-driven soils (530.45 $\text{mg}\cdot\text{kg}^{-1}$) and fluvial-facies-driven soils (560.91 $\text{mg}\cdot\text{kg}^{-1}$), with the remaining
 189 lithologies showing intermediate values. Zn also varied among lithologies, with the highest mean content in acidic
 190 metamorphic rocks (30.79 $\text{mg}\cdot\text{kg}^{-1}$), which was significantly higher than acidic igneous rocks (25.27 $\text{mg}\cdot\text{kg}^{-1}$) and fluvial
 191 facies rocks (25.10 $\text{mg}\cdot\text{kg}^{-1}$), while eolian facies, clastic sedimentary, and carbonate rocks did not differ significantly from
 192 acidic metamorphic rocks or the lower group. For V, acidic-metamorphic-derived soils (63.67 $\text{mg}\cdot\text{kg}^{-1}$) were significantly
 193 higher than fluvial facies, acidic igneous, and clastic sedimentary derived soils, whereas eolian facies rocks and carbonate
 194 rocks showed intermediate levels and were not significantly different from acidic metamorphic rocks or the lower group.



195

196 **Figure 4.** Variability in soil micronutrient contents (Fe, Mn, Zn, V) across Tibetan lithological classes. Boxplots show the data
 197 distributions for each lithological classes. Within each plot, the boxes represent the interquartile range (IQR), the horizontal lines within
 198 boxes indicate the median values, and black dots denote the mean values. The whiskers extend to 1.5 times the IQR. The surrounding
 199 shaded violin shapes indicate the kernel density distribution of the data. Lowercase letters denote significance groups from Tukey's HSD
 200 multiple comparisons ($\alpha = 0.05$): groups sharing at least one letter do not differ significantly, whereas groups with no letters in common
 201 differ significantly (e.g., "ab" is not different from "a" or "b"). Abbreviations of lithological classes: IA = acidic igneous rock, MA = acidic
 202 metamorphic rock, SC = clastic sedimentary rock, SO = carbonate rock, UE = eolian facies rock, UF = fluvial facies rock.

203

3.4 Drivers of soil micronutrient pattern

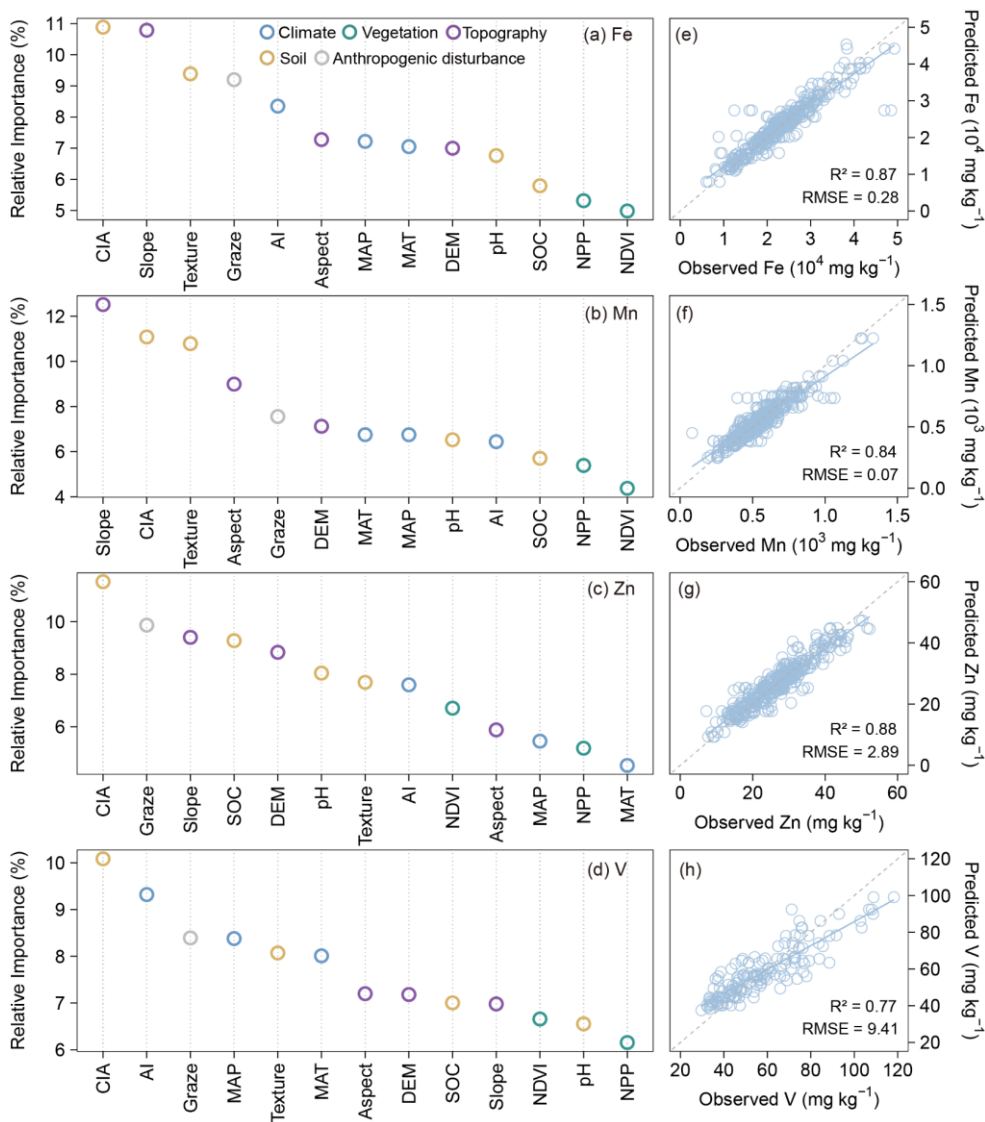
204

Relative importance analysis was conducted for five predictor groups, including climate, vegetation, soil covariates,
 205 topography, and grazing disturbances. The rankings show clear element-specific controls (**Fig. 5a-d**). Soil covariates were
 206 the primary contributors to the spatial variation of micronutrient contents, followed by topographic and climatic factors,
 207 whereas vegetation and anthropogenic disturbance had relatively minor effects. Among all predictors, CIA, slope, and soil
 208 texture exhibited the highest importance, indicating that weathering intensity, terrain, and soil physical structure are the
 209 dominant controls on the spatial distribution of soil micronutrients. Specifically, CIA emerged as the dominant factor for Fe,
 210 Zn, and V. Topographic factors (slope) primarily influenced Mn.

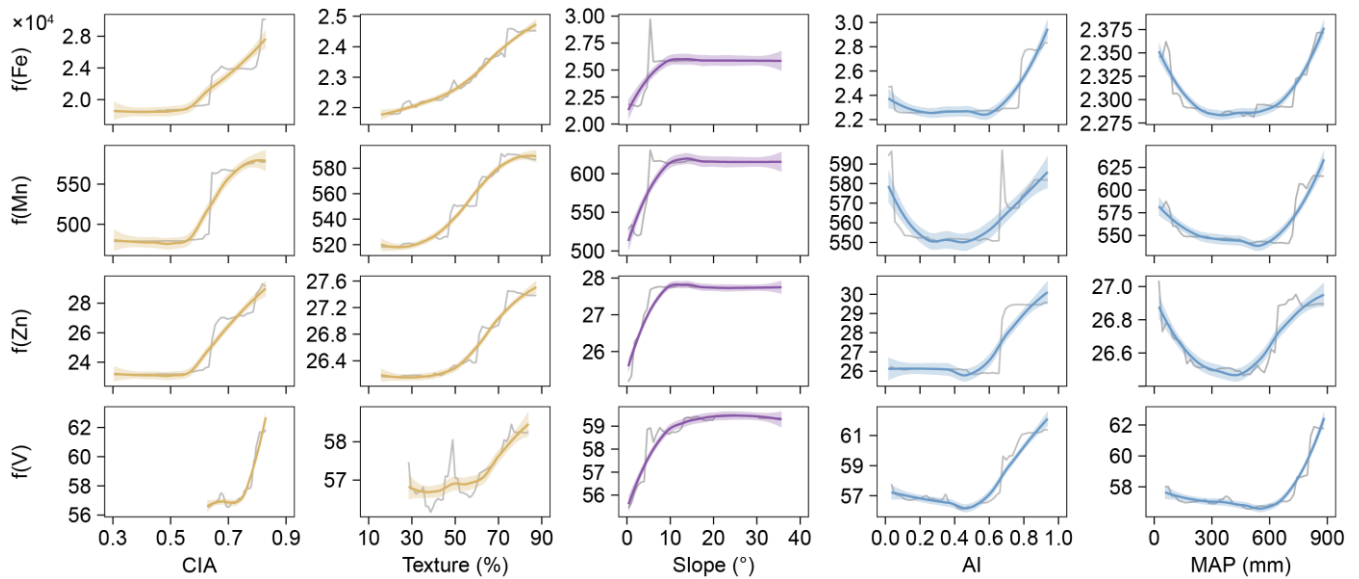
211

The partial dependence plots illustrated the nonlinear responses of four soil micronutrients (Fe, Mn, Zn, and V) to five key
 212 environmental variables (**Fig. 6**). Overall, the effects of CIA, soil texture, slope, and moisture varied substantially among
 213 elements. CIA showed a generally positive relationship with most micronutrients, which increased markedly when chemical
 214 index of alteration exceeded approximately 0.5. Soil texture exerted a moderate positive influence on micronutrients. In
 215 contrast, slope exhibited a saturating effect—nutrient concentrations rose sharply at low slope angles ($<10^\circ$) and plateaued
 216 thereafter—highlighting the limited accumulation potential on steeper terrains. The aridity index demonstrated a clear

217 U-shaped pattern for most micronutrients, with relatively low concentrations under intermediate aridity. Four micronutrients
 218 exhibited a typical U-shaped relationship with mean annual precipitation, showing higher contents in both low and high
 219 precipitation zones, and a clear trough in the intermediate range (approximately 300-500 millimeters). This pattern aligned
 220 closely with responses to drought indices, confirming shared moisture sensitivity. Collectively, these patterns emphasize that
 221 soil micronutrient distributions across the Tibetan Plateau are strongly shaped by interactions among chemical weathering
 222 intensity, soil physical properties, and climatic aridity.



223
 224 **Figure 5.** Relative importance of biotic and abiotic factors for soil micronutrients (Fe, Mn, Zn, V) on the Tibetan Plateau (a-d).
 225 Relationship between observed and predicted values of soil micronutrients (Fe, Mn, Zn, V) on the Tibetan Plateau based on the Random
 226 Forest model (e-h). The blue solid line represents the fitted relationship using ordinary least squares regression, while the gray dashed line
 227 indicates the 1:1 line between observed and predicted values.



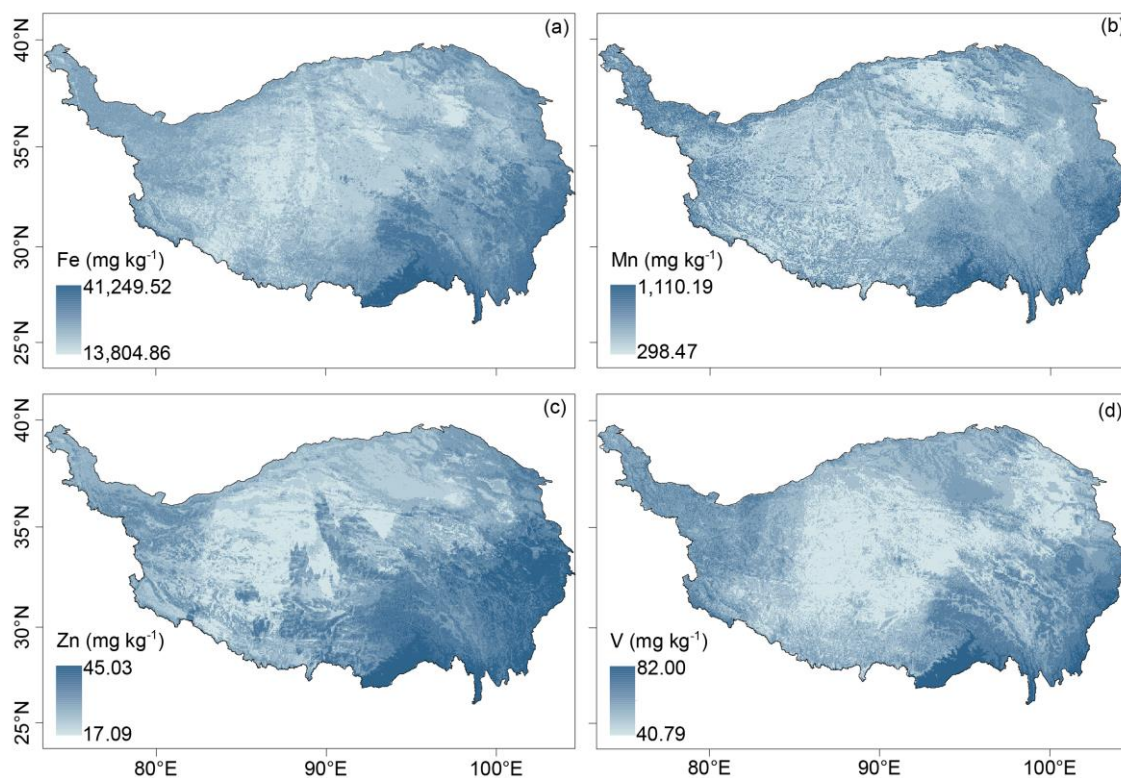
228
 229 **Figure 6.** Partial dependence of four soil micronutrients (Fe, Mn, Zn, V) on five predictive variables: chemical index of alteration (CIA),
 230 Texture, Slope, aridity index (AI) and mean annual precipitation (MAP). Gray lines represent the original partial dependence, while
 231 smoothed fits for each micronutrient are shown as colored lines. Shaded areas represent the 95% confidence intervals.

232 3.5 Soil micronutrients maps

233 The random forest (RF) models exhibited strong overall predictive performance for soil micronutrient contents across the
 234 Tibetan Plateau, with varying accuracies among elements (**Fig. 5e-h**). The models for Fe, Mn, and Zn performed best, with
 235 R^2 values ranging from 0.84 to 0.88 and relatively low RMSE, indicating high consistency between observed and predicted
 236 values. In particular, Zn ($R^2 = 0.88$) and Fe ($R^2 = 0.87$) achieved the highest predictive accuracy, suggesting that their spatial
 237 variability is well captured by the selected environmental predictors. Mn ($R^2 = 0.84$) also showed strong model fits,
 238 reflecting robust representation of their spatial patterns. The V models displayed slightly lower but still acceptable
 239 performance ($R^2 = 0.77$), implying that additional predictors may be required to fully capture their local variability. Overall,
 240 these results demonstrate that the random forest models effectively predict the spatial distributions of major soil
 241 micronutrients, with particularly high reliability for Fe, Mn, and Zn.

242 **Figure 7** illustrates the spatial patterns of soil micronutrients (Fe, Mn, Zn, and V) across the Tibetan Plateau, as predicted by
 243 random forest models. The resulting maps reveal significant spatial heterogeneity of these elements. The highest contents of
 244 Fe are primarily located in the southeastern region, the southern margins, and parts of the western plateau. Mn shows a
 245 distinct gradient, with contents increasing from northeast to southwest. Predicted Mn values range from 298.47 to 1,110.19
 246 $\text{mg}\cdot\text{kg}^{-1}$, and the areas with the highest Mn contents are mainly distributed in the humid southeastern and southern parts of
 247 the plateau. Zn displays relatively high contents in the central-eastern region and along certain western edges of the plateau,
 248 with predicted values ranging from 17.09 to 45.03 $\text{mg}\cdot\text{kg}^{-1}$. Predicted V contents ranged from 40.79 to 82.00 $\text{mg}\cdot\text{kg}^{-1}$,
 249 displaying a clear spatial gradient. Higher contents were predominantly found in the southeastern and southern regions of the

250 plateau, where humid climatic conditions and intense chemical weathering promote V enrichment. Moderate levels occurred
251 across the central and eastern plateau, while the lowest concentrations were observed in the arid western and northern areas.



252
253 **Figure 7.** Spatial distribution of soil micronutrients (Fe, Mn, Zn, V) on the Tibetan Plateau.

254 **4 Discussion**

255 We added comparisons of our results with the few available observations on the Tibetan Plateau, as well as broader datasets
256 from other regions, to better place our findings in a wider context (**Table S2**). In terms of data range and mean values, the
257 contents and magnitudes of the soil micronutrients we observed are generally consistent with previous reports from the
258 Plateau and global grassland soils, indicating the reliability of our datasets. For the Plateau, the mean Zn, and V contents in
259 this study were slightly lower (**Fig. S2**). These discrepancies are more likely due to differences in study regions. Our
260 sampling covered a much broader area, whereas previous studies focused mainly on local regions such as the Heihe Basin
261 (Bu et al., 2016). Given the substantial spatial heterogeneity of soil micronutrients across the Tibetan Plateau, such
262 differences are expected and further highlight the necessity of exploring soil micronutrient patterns at the plateau scale.

263 The vegetation-type contrasts likely reflect ecosystem controls on topsoil (0-10 cm) geochemistry (**Fig. 3**). These contrasts
264 are consistent with ecosystem-mediated controls on topsoil geochemistry, where denser vegetation generally enhances
265 near-surface nutrient cycling through greater biomass inputs, rhizosphere processes, and organic matter accumulation
266 (Hinsinger, 2000). Increased organic inputs and reactive organo-mineral associations can promote retention of Fe, Mn, and

267 Zn and, indirectly, V that is often associated with Fe-bearing phases (Lehmann et al., 2015). In contrast, arid steppe and
268 desert systems typically exhibit weaker soil development and lower organic inputs, reducing reactive surfaces and binding
269 sites for micronutrients, resulting in lower surface pools (Kabata-Pendias, 2010). Cropland tends to show intermediate levels,
270 likely reflecting mixing within the plough layer and partial homogenization of surface concentrations (Alloway, 2008).
271 Lithological class imposes a first order control on surface soil micronutrient variability (**Fig. 4**), consistent with the
272 well-established role of parent material in determining baseline micronutrient pools through differences in primary mineral
273 assemblages and weathering products. In our dataset, acidic metamorphic-derived soils are consistently enriched in Fe, Mn,
274 Zn, and V relative to several other lithologies, whereas acidic igneous and fluvial facies substrates tend to show lower
275 contents, with carbonate, eolian facies, and clastic sedimentary rocks generally occupying intermediate levels. Such contrasts
276 are expected where lithology governs not only the supply of Fe and Mn-bearing minerals but also the abundance of
277 secondary oxides and clay surfaces formed during pedogenesis, which strongly influence trace-element retention and
278 depletion intensity at regional scales (Lara et al., 2018; Spinola et al., 2022). The coherent behaviour of V alongside Fe is
279 also mechanistically plausible because vanadate is efficiently retained by Fe and Mn oxides, making V distributions closely
280 coupled to the abundance and reactivity of these mineral phases (Abernathy et al., 2022; Larsson et al., 2017).

281 The distribution of soil micronutrients across the Tibetan Plateau demonstrates significant spatial heterogeneity (**Figs. 2 and**
282 **7**), aligning with patterns observed in Europe for elements such as Zn (Van et al., 2023). This variability is predominantly
283 governed by the interactions among soil, topography, and climate (**Figs. 5a-d and 6**). Soils act as the principal sink for
284 micronutrients entering the terrestrial environment through both natural processes and anthropogenic inputs. Consistent with
285 continental-scale assessments, clay content emerged as the dominant control on the spatial distribution of soil Zn in Europe,
286 with coarse-textured soils showing markedly lower Zn concentrations (Van et al., 2023). Similar texture effects have been
287 reported for other elements: soil Cu is positively related to clay and negatively related to sand (Ballabio et al., 2018),
288 sensitivity analyses show that soil Se increases with increasing clay (Jones et al., 2017), whereas surface-soil Hg decreases
289 once sand exceeds ~30 % (Ballabio et al., 2021). These patterns agree with our observation that ecosystems developed on
290 coarse substrates contain the lowest levels of micronutrients. This is because clay serves as an adsorption site for metal
291 elements, whereas sandy soils are relatively weak adsorbents for micronutrients (Mesquita, 1998). In poorly developed soils
292 with low clay content, such as those in arid climates, the lack of capacity to retain soil organic matter leads to a significant
293 reduction in the amount of micronutrients, making them less likely to accumulate (Moreno-Jimenez et al., 2019). In addition
294 to soil covariates, factors such as topography also play a significant role in the micronutrient content of surface soils on the
295 Tibetan Plateau. Accumulated local effect (ALE) curves indicate pronounced, nonlinear elevation responses in soil
296 micronutrients, with Fe and Mn generally decreasing with elevation, whereas Zn and V show threshold-like behaviour,

297 remaining relatively stable at mid-elevations but changing sharply at higher elevations (**Fig. S3**). Contents of Fe, Mn, Zn,
298 and V increased with slope steepness, particularly below 10°. This pattern suggests that topography governs both physical
299 and chemical soil-forming processes by controlling erosion, leaching, and moisture dynamics (Jenny, 1941; Montgomery,
300 2007). Steeper slopes enhance runoff and erosion, removing fine particles enriched in Fe and Mn oxides and promoting
301 elemental redistribution along hillslopes, while also accelerating bedrock weathering and releasing lithogenic elements such
302 as Fe and V (Yoo et al., 2006). In contrast, gentler slopes favor organic matter accumulation and reducing conditions that can
303 immobilize or leach redox-sensitive elements. Overall, slope-driven variations in hydrology, weathering, and redox status
304 collectively shape the spatial heterogeneity of soil micronutrients across the Plateau (Quesada et al., 2010).

305 Notably, precipitation emerges as the primary predictor for micronutrients such as Fe, Mn, Zn, and V, with all elements
306 exhibiting characteristic U-shaped responses, with minima occurring at 300-500 mm. This pattern likely reflects distinct
307 weathering regimes across precipitation gradients. In arid regions (<300 mm), physical weathering processes, including
308 freeze-thaw fracturing and aeolian erosion, predominate, allowing micronutrients to accumulate near the surface due to
309 evaporation effects (Pachauri et al., 2014; Moreno-Jimenez et al., 2023). In transitional precipitation regimes (300-500 mm),
310 intensified chemical weathering occurs; however, leaching fluxes surpass the rates of parent material weathering, leading to
311 soil elemental depletion (Anderson, 2019; Bluth et al., 1994; Hartmann et al., 2014). In humid regions (>500 mm), enhanced
312 chemical weathering results in the formation of secondary clay minerals (e.g., montmorillonite, illite), whose negatively
313 charged surfaces facilitate elemental retention through ionic adsorption and co-precipitation mechanisms (Alloway, 2009).

314 To further verify these nonlinear effects, accumulated local effects analyses were performed and revealed consistent
315 U-shaped responses for Fe, Mn, Zn, and V, confirming the robustness of the partial dependence results (**Fig. S4**). This pattern
316 likely reflects a trade-off between weathering intensity, leaching losses, and elemental retention under contrasting
317 hydrological conditions. Additionally, MAP showed a significant positive correlation with CIA (**Fig. S5**), indicating that
318 higher precipitation enhances chemical weathering. However, this relationship alone does not fully explain the observed
319 U-shaped nutrient responses, as direct indicators of leaching fluxes and mineral retention are lacking. We therefore consider
320 this U-shaped pattern, supported by multiple lines of evidence, as an open question for future investigation, emphasizing the
321 need for complementary datasets (e.g., redox status, mineral composition) to refine its mechanistic interpretation. Although
322 lithological differences are detectable for some elements, they do not alter the overall spatial patterns (**Fig. 4**). In summary,
323 lithology modulates the baseline levels of certain micronutrients but is not the dominant factor shaping their regional
324 distributions, which are more strongly governed by external environmental drivers such as climate, weathering intensity,
325 sediment transport, and biotic cycling.

326 Our findings suggest that the aridity index is a significant determinant of soil micronutrient distribution. Specifically,
327 elemental contents tend to decrease when the aridity index falls below a certain threshold (**Fig. 6**). This trend likely reflects
328 reduced input or retention of elements under arid conditions. Grouped comparisons across aridity classes (humid, dry
329 sub-humid, semi-arid, arid, and hyper-arid) were performed. The results show that the medians and means of Fe, Mn, Zn,
330 and V decrease with increasing aridity (**Fig. S6**). Drought conditions may modify soil redox states, thereby influencing
331 element speciation, adsorption capacity, mobility, and ultimately, leaching behavior (Brady et al., 2016; Loveland et al., 2003;
332 Carter et al., 1995). Also, arid environments may indirectly impact micronutrients through alterations in soil pH and soil
333 organic matter content (Moreno-Jimenez et al., 2019). Previous research has shown that droughts induced by climate change
334 can restrict the availability of essential micronutrients, such as iron and zinc (Moreno-Jimenez et al., 2019; Bista et al., 2018).
335 This limitation, along with other adverse effects like diminished water availability, poses substantial threats to vital
336 ecological processes and services in drylands, including food production (Gupta et al., 2008; Graham, 1991). Furthermore,
337 ongoing regional warming and associated hydroclimatic shifts may interact with hydrology and redox processes,
338 organic-matter cycling, and vegetation patterns, thereby altering the availability and spatial variability of certain
339 micronutrients (Myers et al., 2014; Pachauri et al., 2014).

340 Multiple biogeochemical processes are sensitive to micronutrient availability. Biological nitrogen fixation relies on Mo and
341 Fe as essential cofactors of nitrogenase, while the methane cycle depends on Ni and Cu through their roles in
342 methanogenesis and methane oxidation, respectively (Thauer et al., 2019; Stefan et al., 2020). Permafrost thaw and
343 thermokarst development can further activate Fe-Mn redox cycling, altering metal mobility (Chauhan et al., 2024).
344 Collectively, soil micronutrients depletion may cascade through nutrient cycling and ecosystem feedbacks, amplifying the
345 impacts of ongoing environmental change across the Plateau.

346 **5 Uncertainty**

347 Although the laboratory XRF measurements used in this study were validated against ICP-MS and generally showed strong
348 correlations, several limitations should be noted. For Fe, Mn, and V, the two methods produced highly consistent results,
349 supporting the robustness of the dataset. In contrast, Zn exhibited systematic deviations from the 1:1 line, with XRF tending
350 to slightly underestimate contents relative to ICP-MS (**Fig. S1**). These deviations likely arise from element-specific detection
351 sensitivities of XRF. To address this, we calibrated Zn, using the regression relationships between the two methods and then
352 repeated spatial mapping. The results before and after calibration were not significantly different, confirming that these
353 deviations do not affect our main findings (**Figs. S7 and S8**). Furthermore, the primary scientific purpose of this dataset is to

354 characterize spatial patterns, ecological gradients, and multivariate relationships across the Plateau, rather than to provide
355 ultra-precise quantification of element contents at the individual-sample level. For these objectives, XRF-derived contents,
356 supported by calibration, cross-validation, and transparent uncertainty reporting, provide reliable and ecologically
357 interpretable information. Nonetheless, we acknowledge that incorporating ICP-based measurements on a larger sample set
358 would further strengthen the accuracy of the dataset, and future efforts should consider combining multiple analytical
359 approaches to minimize methodological uncertainties.

360 Our random forest regression models demonstrated robust predictive capability (e.g. cross-validated R^2 range from 0.65 to
361 0.77 for Fe, Mn, and Zn; **Table S3**), V exhibit weaker predictive performance ($R^2 = 0.39$). The spatial predictions inevitably
362 contain uncertainties arising from both the Random Forest model and the input datasets. Model-based uncertainty was
363 quantified as the inter-tree variance among predictions (RF-SD; **Fig. S9**), while additional uncertainty may stem from sparse
364 meteorological observations and limited soil sampling across the Tibetan Plateau. Large regions in the west (including parts
365 of the Changtang Plateau and Ngari) are sparsely inhabited and difficult to access, with extensive high-elevation terrain and
366 access restrictions that constrain fieldwork. Consequently, model estimates in these areas are supported by fewer
367 observations and should be interpreted with greater caution. We therefore recommend that users consider the accompanying
368 uncertainty layer when applying the gridded products, especially for analyses focusing on the western Plateau or on
369 fine-scale local interpretation. Nevertheless, model accuracy could be further improved to more extensive field sampling and
370 refinement of input data. Specifically, targeted collection of soil micronutrient data and associated covariates in
371 underrepresented high-altitude regions of the Tibetan Plateau is necessary to address existing spatial gaps. Additionally,
372 systematic reduction of uncertainties inherent in gridded environmental datasets is essential, as these uncertainties propagate
373 errors into micronutrient predictions. Continued advancement in both field observations and foundational geospatial dataset
374 is crucial for improving the reliability of regional-scale element mapping.

375 We note that the reported contents represent a fixed-depth (0-10 cm) surface layer, which may correspond to different
376 dominant horizons among land uses (organic-rich surface in some forests, mineral topsoil in grasslands/meadows, and the
377 plough layer in croplands). Users should consider this context when applying the dataset, especially for process inference or
378 when comparing across ecosystems with contrasting surface horizons. Where applications require deeper profiles or
379 horizon-specific interpretation, we recommend integrating our maps with local profile data. Because croplands occupy a very
380 small fraction of the Plateau and are represented by a limited number of samples in our area-weighted design,
381 cropland-related results should be interpreted primarily as a cross-ecosystem contrast at the plateau scale. Users addressing
382 cropland-specific questions are advised to use these values with caution and, where possible, complement them with targeted
383 cropland sampling or independent field observations.

384 **6 Data availability**

385 The gridded soil micronutrient (Fe, Mn, Zn, and V) maps for Tibetan Plateau can be downloaded from [https://doi.org/](https://doi.org/10.11888/Terre.tpdc.303242)
386 10.11888/Terre.tpdc.303242 (Huo et al., 2025).

387 **7 Conclusions**

388 This study delivers a comprehensive assessment of spatial distribution patterns for four soil micronutrients (Fe, Mn, Zn, and
389 V) across the Tibetan Plateau, revealing pronounced regional-scale heterogeneity. Soil covariates were the primary
390 contributors to the spatial variation of micronutrient contents, followed by topographic and climatic factors, whereas
391 vegetation and grazing disturbance had relatively minor effects. These findings highlight the coupled effects of climate,
392 vegetation, and parent material on micronutrient biogeochemical cycling within the complex environmental context of the
393 Tibetan Plateau. Using five predictor groups (climate, vegetation, soil covariates, topography, and grazing disturbances), we
394 generated high-resolution spatial maps for key soil micronutrients (Fe, Mn, Zn, and V) via machine learning. These maps
395 provide validated initial conditions for process-based models simulating micronutrient cycling, advances understanding of
396 elemental distribution in alpine ecosystems.

397 **Author contributions.**

398 JZ conceived the study. HY conducted the field survey and was responsible for data collection and processing. HY prepared
399 the manuscript with contributions from all co-authors.

400 **Competing interests.**

401 The contact author has declared that none of the authors has any competing interests.

402 **Acknowledgements.**

403 This study was supported by the Second Tibetan Plateau Scientific Expedition and Research Program (2022QZKK0101),
404 National Natural Science Foundation of China (42471159), and Chinese Academy of Sciences (CAS) Project for Young
405 Scientists in Basic Research (YSBR-037).

406 **Appendix A: Supplementary material**

407 **Appendix B: Metadata**

408 **References**

- 409 Abernathy, M. J., Schaefer, M. V., Ramirez, R., Garniwan, A., Lee, I., Zaera, F., Polizzotto, M. L., and Ying, S. C.: Vanadate
410 retention by iron and manganese oxides, *ACS Earth and Space Chemistry*, 6, 2041-2052,
411 <https://doi.org/10.1021/acsearthspacechem.2c00116>, 2022.
- 412 Alloway, B. J.: Zinc in soils and crop nutrition, 2nd edn., International Zinc Association (IZA) and International Fertilizer
413 Industry Association (IFA), Brussels and Paris, 2008.
- 414 Alloway, B. J.: Soil factors associated with zinc deficiency in crops and humans, *Environmental Geochemistry and Health*,
415 31, 537-548, <https://doi.org/10.1007/s10653-009-9255-4>, 2009.
- 416 Anderson, S. P.: Breaking it down: Mechanical processes in the weathering engine, *Elements: An International Magazine of*
417 *Mineralogy, Geochemistry, and Petrology*, 15, 247-252, <https://doi.org/10.2138/gselements.15.4.247>, 2019.
- 418 Bluth, G. J., and Kump, L. R.: Lithologic and climatologic controls of river chemistry, *Geochimica et Cosmochimica Acta*,
419 58, 2341-2359, [https://doi.org/10.1016/0016-7037\(94\)90015-9](https://doi.org/10.1016/0016-7037(94)90015-9), 1994.
- 420 Ballabio, C., Jiskra, M., Osterwalder, S., Borrelli, P., Montanarella, L., and Panagos, P.: A spatial assessment of mercury
421 content in the European Union topsoil, *Science of the Total Environment*, 769, 144755, [https://doi.org/](https://doi.org/10.1016/j.scitotenv.2020.144755)
422 [10.1016/j.scitotenv.2020.144755](https://doi.org/10.1016/j.scitotenv.2020.144755), 2021.
- 423 Ballabio, C., Panagos, P., Lugato, E., Huang, J. H., Orgiazzi, A., Jones, A., Fernández-Ugalde, O., Borrelli, P., and
424 Montanarella, L.: Copper distribution in European topsoils: An assessment based on LUCAS soil survey, *Science of the*
425 *Total Environment*, 636, 282-298, <https://doi.org/10.1016/j.scitotenv.2018.04.268>, 2018.
- 426 Bista, D. R., Heckathorn, S. A., Jayawardena, D. M., Mishra, S., and Boldt, J. K.: Effect of drought and carbon dioxide on
427 nutrient uptake and levels of nutrient-uptake proteins in roots of barley, *American Journal of Botany*, 107, 1401-1409,
428 <https://doi.org/10.1002/ajb2.1542>, 2018.
- 429 Brady, N. C. and Weil, R. R.: *The nature and properties of soils*, Pearson Education, Boston, 1104 pp., 2016.
- 430 Bu, J. W., Sun, Z. Y., Zhou, A. G., Xu, Y. N., Ma, R., Wei, W. H., and Liu, M.: Heavy Metals in Surface Soils in the Upper
431 Reaches of the Heihe River, Northeastern Tibetan Plateau, China, 13, <https://doi.org/10.3390/ijerph13030247>, 2016.
- 432 Cardon, Z. G., Stark, J. M., Herron, P. M., and Rasmussen, J. A.: Sagebrush carrying out hydraulic lift enhances surface soil
433 nitrogen cycling and nitrogen uptake into inflorescences, *Proceedings of the National Academy Sciences of the United*
434 *States of America*, 110, 18988-18993, <https://doi.org/10.1073/pnas.1311314110>, 2013.
- 435 Carter, M. R. and Stewart, B. A.: *Structure and organic matter storage in agricultural soils*, CRC Press, Boca Raton, 304 pp.,
436 1995.

437 Chauhan, A., Patzner, M. S., Bhattacharyya, A., Borch, T., Fischer, S., Obst, M., Thomasarrigo, L. K., Kretzschmar, R.,
438 Mansor, M., Bryce, C., Kappler, A., and Joshi, P.: Interactions between iron and carbon in permafrost thaw ponds,
439 Science of the Total Environment, 946, 174321, <https://doi.org/10.1016/j.scitotenv.2024.174321>, 2024.

440 Cheng, C. J., He, N. P., Li, M. X., Xu, L., Cai, W. X., Li, X., Zhao, W. W., Li, C., and Sun, O. J.: Plant species richness on
441 the Tibetan Plateau: patterns and determinants, Ecography, 2023, <https://doi.org/10.1111/ecog.06265>, 2022.

442 Cheng, F. T., Chen, D. L., Wang, B., Ou, T. H., and Lu, M. Q.: Human-induced warming accelerates local evapotranspiration
443 and precipitation recycling over the Tibetan Plateau, Communications Earth Environment, 388,
444 <https://doi.org/10.1038/s43247-024-01537-8>, 2024.

445 Chen, J. H., Wang, Y. F., Sun, J., Zhang, J. X., Zhang, J. T., Wang, Y. X., Zhou, T. C., Huo, H. Y., and Liang, E. Y.: Linking
446 ecosystem service benefit and grazing prohibition intensity can better optimize fence layout in northern Tibet, Land
447 Degradation Development, 34, 2038-2051, <https://doi.org/10.1002/ldr.4587>, 2023.

448 Dallman, P. R.: Biochemical basis for the manifestations of iron deficiency, Annual Review of Nutrition, 6, 13-40,
449 <https://doi.org/10.1146/annurev.nu.06.070186.000305>, 1986.

450 Dijkshoorn, J. A., van Engelen, V. W. P., and Huting, J. R. M.: Soil and landform properties for LADA partner countries
451 (Argentina, China, Cuba, Senegal and The Gambia, South Africa and Tunisia), ISRIC Report 2008/06 and GLADA
452 Report 2008/03, ISRIC-World Soil Information and FAO, Wageningen, 23 pp., 2008.

453 Dijkstra, J. J., Meeussen, J. C. L., and Comans, R. N. J.: Leaching of heavy metals from contaminated soils: an experimental
454 and modeling study. Environmental Science & Technology, 38, 4390-4395, <https://doi.org/10.1021/es049885v>, 2004.

455 Dong, K., Li, W. J., Tang, Y. L., Ma, S. H., and Jiang, M. L.: Co-limitation of N and P is more prevalent in the
456 Qinghai-Tibetan Plateau grasslands, Frontiers in Plant Science, 14, 1140462, <https://doi.org/10.3389/fpls.2023.1140462>,
457 2023.

458 Du, Z. Y., Cai, Y. J., Yan, Y., and Wang, X. D.: Embedded rock fragments affect alpine steppe plant growth, soil carbon and
459 nitrogen in the northern Tibetan Plateau, Plant and Soil, 420, 79-92, <https://doi.org/10.1007/s11104-017-3376-9>, 2017.

460 Fageria, N. K., Baligar, V. C., and Clark, R. B.: Micronutrients in crop production. Advances in Agronomy, 77, 185-268,
461 [https://doi.org/10.1016/S0065-2113\(02\)77015-6](https://doi.org/10.1016/S0065-2113(02)77015-6), 2002.

462 Fedo, C. M., Nesbitt, H. W., and Young, G. M.: Unraveling the effects of potassium metasomatism in sedimentary rocks and
463 paleosols, with implications for paleoweathering conditions and provenance, Geology, 23, 921-924,
464 [https://doi.org/10.1130/0091-7613\(1995\)023<0921:UTEOPM>2.3.CO;2](https://doi.org/10.1130/0091-7613(1995)023<0921:UTEOPM>2.3.CO;2), 1995.

465 Fischer, W. W., Hemp, J., and Johnson, J. E.: Manganese and the evolution of photosynthesis, Origins of Life and Evolution
466 of Biospheres, 45, 351-357, <https://doi.org/10.1007/s11084-015-9442-5>, 2015.

467 Graham, T. W.: Trace element deficiencies in cattle, *Veterinary Clinice of North America-Food Animal Practice*, 7, 153-215,
468 [https://doi.org/10.1016/S0749-0720\(15\)30816-1](https://doi.org/10.1016/S0749-0720(15)30816-1), 1991.

469 Gupta, U. C., Wu, K., and Liang, S.: Micronutrients in soils, crops, and livestock. *Earth Science Frontiers*, 15, 110-125,
470 2008.

471 Guan, Z. H., Li, X. G., and Wang, L.: Heavy metal enrichment in roadside soils in the eastern Tibetan Plateau,
472 *Environmental Science and Pollution Research*, 25, 7625-7637, <https://doi.org/10.1007/s11356-017-1094-8>, 2017.

473 Han, D. L., Huang, J. P., Ding, L., Zhang, G. L., Liu, X. Y., Li, C. Y., and Yang, F.: Breaking the Ecosystem Balance Over the
474 Tibetan Plateau, *Earth's Future*, 10, <https://doi.org/10.1029/2022EF002890>, 2022.

475 Hartmann, J., Moosdorf, N., Lauerwald, R., Hinderer, M., and West, A. J.: Global chemical weathering and associated
476 P-release-The role of lithology, temperature and soil properties, *Chemical Geology*, 363, 145-163,
477 <https://doi.org/10.1016/j.chemgeo.2013.10.025>, 2014.

478 Hartmann, M., and Six, J.: Soil structure and microbiome functions in agroecosystems, *Nature Reviews Earth &*
479 *Environment*, 4, 4-18, <https://doi.org/10.1038/s43017-022-00366-w>, 2023.

480 Hänsch, R., and Mendel, R. R.: Physiological functions of mineral micronutrients (Cu, Zn, Mn, Fe, Ni, Mo, B, Cl), *Current*
481 *Opinion in Plant Biology*, 12, 259-266, <https://doi.org/10.1016/j.pbi.2009.05.006>, 2009.

482 Hinsinger, P.: Bioavailability of trace elements as related to root-induced changes in the rhizosphere, *Trace Elements in the*
483 *Rhizosphere*, 25-41, <http://dx.doi.org/10.1201/9781420039993.ch2>, 2001.

484 Hou, X. Y. (Ed.): *Atlas of vegetation of China (1:1,000,000)*, Science Press, Beijing, 2019.

485 Jenny, H.: *Factors of Soil Formation: A System of Quantitative Pedology*, McGraw-Hill, New York, 1941.

486 Jones, D. L., Cross, P., Withers, P. J., DeLuca, T. H., Robinson, D. A., Quilliam, R. S., Harris, I. M., Chadwick, D. R., and
487 Edwards-Jones, G.: Nutrient stripping: The global disparity between food security and soil nutrient stocks, *Journal of*
488 *Applied Ecology*, 50, 851-862, <https://doi.org/10.1111/1365-2664.12089>, 2013.

489 Jones, G. D., Droz, B., Greve, P., Gottschalk, P., Poffet, D., McGrath, S. P., Seneviratne, S. I., Smith, P., and Winkel, L. H. E.:
490 Selenium deficiency risk predicted to increase under future climate change, *Proceedings of the National Academy of*
491 *Sciences of the United States of America*, 114, 2848-2853, <https://doi.org/10.1073/pnas.1611576114>, 2017.

492 Kabata-Pendias, A.: *Trace elements in soils and plants*, 4th edn., CRC Press, Boca Raton, FL, USA, 2011.

493 Lara, M. C., Buss, H. L., and Pett-Ridge, J. C.: The effects of lithology on trace element and REE behavior during tropical
494 weathering, *Chemical Geology*, 500, 88-1020, <https://doi.org/10.1016/j.chemgeo.2018.09.024>, 2018.

495 Larsson, M. A., Persson, I., Sjoestedt, C., and Gustafsson, J. P.: Vanadate complexation to ferrihydrite: X-ray absorption
496 spectroscopy and CD-MUSIC modelling, *Environmental Chemistry*, 14, 141-150, <https://doi.org/10.1071/EN16174>,
497 2017.

498 Lehmann, J., and Kleber, M.: The contentious nature of soil organic matter, *Nature*, 528, 60-68, [https://doi.org/](https://doi.org/10.1038/nature16069)
499 [10.1038/nature16069](https://doi.org/10.1038/nature16069), 2015.

500 Lemière, B.: A review of pXRF (field portable X-ray fluorescence) applications for applied geochemistry, *Journal of*
501 *Geochemical Exploration*, 188, 350-363, <https://doi.org/10.1016/j.gexplo.2018.02.006>, 2018.

502 Lindsay, W. L.: *Chemical equilibria in soils*, John Wiley and Sons Ltd., New York, 449 pp., 1979.

503 Loveland, P. and Webb, J.: Is there a critical level of organic matter in the agricultural soils of temperate regions: a review,
504 *Soil Tillage Research*, 70, 1–18, [https://doi.org/10.1016/S0167-1987\(02\)00139-3](https://doi.org/10.1016/S0167-1987(02)00139-3), 2003.

505 McLennan, S. M.: Weathering and global denudation, *The Journal of Geology*, 101, 295-303, <https://doi.org/10.1086/648222>,
506 1993.

507 Mesquita, M. E.: Copper and zinc competitive adsorption in schistic and granitic acid soils, *Agrochimica*, 42, 235-245, 1998.

508 Montgomery, D. R.: Soil erosion and agricultural sustainability, *Proceedings of the National Academy of Sciences of the*
509 *United States of America*, 104, 13268-13272, <https://doi.org/10.1073/pnas.0611508104>, 2007.

510 Moreno-Jimenez, E., Maestre, F. T., Flagmeier, M., Guirado, E., Berdugo, M., Bastida, F., Dacal, M., Díaz-Martínez, P.,
511 Ochoa-Hueso, R., Plaza, C, Rillig, MC., Crowther, T. W., and Delgado-Baquerizo, M.: Soils in warmer and less
512 developed countries have less micronutrients globally, *Global Change Biology*, 29, 522-532,
513 <https://doi.org/10.1111/gcb.16478>, 2023.

514 Moreno-Jimenez, E., Plaza, C., Saiz, H., Manzano, R., Flagmeier, M., and Maestre, F. T.: Aridity and reduced soil
515 micronutrient availability in global drylands, *Nature Sustainability*, 2, 371-377,
516 <https://doi.org/10.1038/s41893--019-0262-x>, 2019.

517 Mu, C. C., Zhang, F., Mu, M., Chen, X., Li, Z. L., and Zhang, T. J.: Organic carbon stabilized by iron during slump
518 deformation on the Qinghai-Tibetan Plateau, *Catena*, 187, 104282, <https://doi.org/10.1016/j.catena.2019.104282>, 2020.

519 Mu, C. C., Zhang, T. J., Zhao, Q., Guo, H., Zhong, W., Su, H., and Wu, Q.B.: Soil organic carbon stabilization by iron in
520 permafrost regions of the Qinghai-Tibet Plateau, *Geophysical Research Letters*, 43, 10286-10294,
521 <https://doi.org/10.1002/2016GL070071>, 2016.

522 Myers, S. S., Zanobetti, A., Kloog, I., Huybers, P., Leakey, A. D., Bloom, A. J., Carlisle, E., Dietterich, L. H., Fitzgerald, G.,
523 Hasegawa, T., Holbrook, N. M., Nelson, R. L., Ottman, M. J., Raboy, V., Sakai, H., Sartor, K. A., Schwartz, J.,

524 Seneweera, S., Tausz, and M., Usui, Y.: Increasing CO₂ threatens human nutrition, *Nature*, 510, 139-142,
525 <https://doi.org/10.1038/nature13179>, 2014.

526 Nesbitt, H.W., and Young, G.M.: Early Proterozoic climates and plate motions inferred from major element chemistry of
527 lutites, *Nature*, 299, 715-717, <https://doi.org/10.1038/299715a0>, 1982.

528 Ochoa-Hueso, R., Plaza, C., Moreno-Jimenez, E., and Delgado-Baquerizo, M.: Soil element coupling is driven by ecological
529 context and atomic mass, *Ecology Letters*, 24, 319-326, <https://doi.org/10.1111/ele.13648>, 2020.

530 O'Hara, G. W.: Nutritional constraints on root nodule bacteria affecting symbiotic nitrogen fixation: A review, *Australian*
531 *Journal of Experimental Agriculture*, 41, 417-433, <https://doi.org/10.1071/EA00087>, 2001.

532 Pachauri, R. K., Allen, M. R., Barros, V. R., Broome, J., Cramer, W., Christ, R., Church, J. A., Clarke, L., Dahe, Q., and
533 Dasgupta, P.: Climate change 2014: Synthesis report. Contribution of Working Groups I, II and III to the Fifth
534 Assessment Report of the Intergovernmental Panel on Climate Change, IPCC, Geneva, Switzerland, 151 pp., 2014.

535 Pan, J. X., Zhang, X. Y., Liu, S., Liu, N., Liu, M. J., Chen, C., Zhang, X. Y., Niu, S. L., and Wang, J. S.: Precipitation
536 alleviates microbial C limitation but aggravates N and P limitations along a 3000-km transect on the Tibetan Plateau,
537 *Catena*, 247, 108535, <https://doi.org/10.1016/j.catena.2024.108535>, 2024.

538 Piñeiro, G., Perelman, S., Guerschman, J. P., and Paruelo, J. M.: How to evaluate models: Observed vs. predicted or
539 predicted vs. observed? *Ecological Modelling*, 216, 316-322, <https://doi.org/10.1016/j.ecolmodel.2008.05.006>, 2008.

540 Potter, C. S., Randerson, J. T., Field, C. B., Matson, P. A., Vitousek, P. M., Mooney, H. A., and Klooster, S. A.: Terrestrial
541 ecosystem production: A process model based on global satellite and surface data, *Global Biogeochemical Cycles*, 7,
542 811-841, <https://doi.org/10.1029/93GB02725>, 1993.

543 Prestele, R., Alexander, P., Rounsevell, M. D., Arneth, A., Calvin, K., Doelman, J., Eitelberg, D. A., Engström, K., Fujimori,
544 S., Hasegawa, T., Havlik, P., Humpenoeder, F., Jain, A. K., Krisztin, T., Kyle, P., Meiyappan, P., Popp, A., Sands, R. D.,
545 Schaldach, R., Schuengel, J., Stehfest, E., Tabeau, A., Van Meijl, H., Van Vliet, J., Verburg, P. H.: Hotspots of
546 uncertainty in land-use and land-cover change projections: A global-scale model comparison, *Global Change Biology*,
547 22, 3967-3983, <https://doi.org/10.1111/gcb.13337>, 2016.

548 Quesada, C. A., Lloyd, J., Schwarz, M., Patino, S., Baker, T. R., Czimczik, C., Fyllas, N. M., Martinelli, L., Nardoto, G. B.,
549 Schmerler, J., Santos, A. J. B., Hodnett, M. G., Herrera, R., Luizao, F. J., Arneth, A., Lloyd, G., Dezzio, N., Kuhlmann,
550 I., Raessler, M., Brand, W. A., Geilmann, H., Moraes Filho, J. O., Carvalho, F. P., Araujo Filho, R. N., Chaves, J. E.,
551 Cruz Junior, O. F., Pimentel, T. P., and Paiva, R.: Variations in chemical and physical properties of Amazon forest soils
552 in relation to their genesis, *Biogeosciences*, 7, 1515-1541, <https://doi.org/10.5194/bg-7-1515-2010>, 2010.

553 Schmidt, W., Thomine, S., and Buckhout, T. J.: Iron nutrition and interactions in plants, *Frontiers in Plant Science*, 10, 1670,
554 <https://doi.org/10.3389/fpls.2019.01670>, 2020.

555 Simon M. N.: *Inductively Coupled Plasma Mass Spectrometry Handbook*, Blackwell Publishing, Oxford, 2005.

556 Spinola, D., Portes, R., Fedenko, J., Lybrand, R., Dere, A., Biles, F., Trainor, T., Bowden, M. E., and D'Amore, D.:
557 Lithological controls on soil geochemistry and clay mineralogy across Spodosols in the coastal temperate rainforest of
558 southeast Alaska, *Geoderma*, 428, 116211, <https://doi.org/10.1016/j.geoderma.2022.116211>, 2022.

559 Stefan, B., Jiménez-Vicente, E., Echavarri-Erasun, C., and Rubio, L. M.: Biosynthesis of Nitrogenase Cofactors, *Chemical*
560 *Reviews*, 120, 4919-5794, <https://doi.org/10.1021/acs.chemrev.9b00489>, 2020.

561 Stehfest, E., van Zeist, W. J., Valin, H., Havlik, P., Popp, A., Kyle, P., Tabeau, A., Mason-D'Croz, D., Hasegawa, T., Bodirsky,
562 B. L., Calvin, K., Doelman, J. C., Fujimori, S., Humpenoeder, F., Lotze-Campen, H., van Meijl, H., and Wiebe, K.: Key
563 determinants of global land-use projections, *Nature Communications*, 10, 1-10,
564 <https://doi.org/10.1038/s41467-019-09945-w>, 2019.

565 St Clair, S. B. S., and Lynch, J. P.: The opening of Pandora's Box: Climate change impacts on soil fertility and crop nutrition
566 in developing countries, *Plant and Soil*, 335, <https://doi.org/10.1007/s11104-010-0328-z101-115>, 2010.

567 Thauer, P. K.: Methyl (Alkyl)-Coenzyme M Reductases: Nickel F-430-Containing Enzymes Involved in Anaerobic Methane
568 Formation and in Anaerobic Oxidation of Methane or of Short Chain Alkanes, *Biochemistry*, 58, 5198-5220.
569 <https://doi:10.1021/acs.biochem.9b00164>, 2019.

570 Tian, L. M., Zhao, L., Wu, X. D., Hu, G. J., Fang, H. B., Zhao, Y. H., Sheng, Y., Chen, J., Wu, J. C., Li, W. P., Ping, C.L.,
571 Pang, C. L., Pang, Q. Q., Liu, Y., Shi, W., Wu, T. H., and Zhang, X. M.: Variations in soil nutrient availability across
572 Tibetan grassland from the 1980s to 2010s, *Geoderma*, 338, 197-205, <https://doi.org/10.1016/j.geoderma.2018.12.009>,
573 2019.

574 Trabucco, A. and Zomer, R. J.: Global Aridity Index and Potential Evapo-Transpiration (ET₀) Climate Database v2, CGIAR
575 Consortium for Spatial Information (CGIAR-CSI) [data set], <https://cgiaresci.community>, 2018.

576 Van, Eynde. E., Fendrich, A. N., Ballabio, C., and Panagos, P.: Spatial assessment of topsoil zinc concentrations in Europe,
577 *Science of the Total Environment*, 892, 164512, <https://doi.org/10.1016/j.scitotenv.2023.164512>, 2023.

578 White, P. J., and Broadley, M. R.: Biofortifying crops with essential mineral elements. *Trends in Plant Science*, 10, 586-593,
579 <https://doi.org/10.1016/j.tplan ts.2005.10.001>, 2005.

580 Yao, T. D., Thompson, L. G., Mosbrugger, V., Zhang, F., Ma, Y. M., Luo, T. X., Xu, B. Q., Yang, X. X., Joswiak, D. R.,
581 Wang, W. C., Joswiak, M. E., Devkota, L. P., Tayal, S., Jilani, R., Fayziev, R.: Third Pole Environment (TPE),
582 *Environmental Development*, 3, 52-64, <https://doi.org/10.1016/j.envdev.2012.04.002>, 2012.

- 583 Yoo, K., Amundson, R., Mudd, S. M., Sanderman, J., Amundson, R., and Blum, A.: Spatial patterns and controls of soil
584 chemical weathering rates along a transient hillslope, *Earth and Planetary Science Letters*, 288, 184-193,
585 <https://doi.org/10.1016/j.epsl.2009.09.021>, 2006.
- 586 Yu, Y. F., You, Q. L., Zhang, Y. Q., Jin, Z., Kang, S. C., and Zhai, P. M.: Integrated warm-wet trends over the Tibetan Plateau
587 in recent decades, *Journal of Hydrology*, 639, 131599, <https://doi.org/10.1016/j.jhydrol.2024.131599>, 2024.
- 588 Zhang, H., Wang, Z. F., Zhang, Y. L., and Hu, Z. J.: The effects of the Qinghai-Tibet railway on heavy metals enrichment in
589 soils, *Science of the Total Environment*, 439, 240-280, <https://doi.org/10.1016/j.scitotenv.2012.09.027>, 2012.